Solid State Electronics 155 (2019) 111–116

Contents lists available at ScienceDirect

Solid State Electronics

journal homepage: www.elsevier.com/locate/sse

Signatures of induced superconductivity in AlO_x-capped topological heterostructures

Peter Schüffelgen[a,*], Daniel Rosenbach[a], Yuan Pang[b], Jörn Kampmeier[a], Martina Luysberg[a], Lidia Kibkalo[a], Gregor Mussler[a], Dick Veldhuis[c], Alexander Brinkman[c], Li Lu[b], Thomas Schäpers[a], Detlev Grützmacher[a]

[a] Peter Grünberg Institute, Forschungszentrum Jülich & JARA Jülich-Aachen Research Alliance, 52425 Jülich, Germany
[b] Daniel Chee Tsui Laboratory, Beijing National Laboratory for Condensed Matter Physics & Institute of Physics, Chinese Academy of Sciences, Beijing 100190, People's Republic of China
[c] MESA + Institute for Nanotechnology, Interfaces and Correlated Electrons, University of Twente, 7500AE Enschede, The Netherlands

ARTICLE INFO

The review of this paper was arranged by Prof. S. Luryi, J.M. Xu, and A. Zaslavsky

Keywords:
Topological insulator
Induced superconductivity
In situ capping
Molecular beam epitaxy
Majorana

ABSTRACT

In order to access exotic Dirac and Majorana states in (Bi,Sb)-based topological insulators (TIs), the physical surface of those crystals should not be exposed to air. 2–3 nm of *in situ* deposited Al on top of pristine TI thin films immediately oxidizes after taking the sample to ambient conditions. The native AlO_x provides a favorable hard capping, which preserves the topological surface states during *ex situ* device fabrication. Here, we present a process on how to construct superconductor – topological insulator – superconductor (S-TI-S) junctions from *in situ* capped thin films comprised of 15 nm Sb_2Te_3 on top of 6 nm Bi_2Te_3. The thicknesses of the Sb_2Te_3 and the Bi_2Te_3 layer allow us to precisely tune the Fermi level of the upper surface of the Sb_2Te_3 layer. The challenge is to provide a transparent interface between Sb_2Te_3 and the superconductive Nb, while assuring an AlO_x-capped weak link in between two closely separated Nb electrodes. Low temperature experiments on our junctions provide evidence for charge transport mediated by coherent Andreev states. Magnetic field dependent measurements yielded Fraunhofer-like patterns, whose periodicities are in good agreement with the effective areas of the respective junctions. Transmission electron micrographs of the narrowest junction confirm a crystalline and capped weak link. Our results provide the first reported signatures of induced superconductivity in S-TI-S junctions, which are capped by native AlO_x. The presented process allows for accessing S-TI hybrid devices via magnetic flux, while assuring *in situ* conserved weak links. This makes as-prepared junctions a promising platform for proposed flux-controllable Majorana devices.

1. Introduction

Majorana states – exotic quasiparticle excitations in solid states, which can be utilized for quantum computational tasks [1] – are predicted at the interface of topological insulators (TI) and s-wave superconductors (S) [2–4]. As recently demonstrated (Bi,Sb)-based S-TI-S junctions, which had their topological weak link – i.e. the area in between two closely separated superconductive electrodes – capped *in situ*, exhibit signatures of Majorana bound states (MBS) in transport experiments [5]. However, the fabrication process of those devices did not allow for applying magnetic flux to the devices in a controllable manner. Reason is the global stencil mask that was permanently attached to the chip and that has been fully covered by superconductive Nb during fabrication. At low temperatures, Nb turns into a perfect diamagnet, which screens magnetic fluxes. To exploit Majorana devices for flux-controlled tasks [6], the covered stencil mask needs to be removed later or bypassed in advance. In this work, *in situ* capped S-TI-S junctions were fabricated in a straightforward manner, without making use of complex stencil lithography.

The delicate topological surface of our thin film was capped *in situ*, following the pioneering work of Lang et al. [7]. Lang and co-workers showed that the deposition of a thin metallic Al capping layer fulfils the requirements of protecting the topological surface at ambient conditions. Transport experiments on capped *μm*-sized Hall bar devices showed that the pristine surface is protected and signatures of Dirac states were observed in Shubnikov-de Haas oscillations. Whereas in uncapped devices these signatures were absent. In order to protect the topological surface states in *nm*-sized devices for investigating induced

* Corresponding author.
E-mail address: p.schueffelgen@fz-juelich.de (P. Schüffelgen).

https://doi.org/10.1016/j.sse.2019.03.003

Available online 04 March 2019
0038-1101/

superconductivity, we adopt their approach for fabrication of lateral Josephson junctions (JJ).

The deposition of superconductive material defines the most crucial step in fabrication of lateral JJs. The surfaces of uncapped 3D TIs tend to oxidize rather quickly. In some TIs, a drift of the Fermi level indicates chemical reactions at the surface within minutes at ambient conditions [8,9]. To guarantee a high interface transparency between a superconductive electrode and the topological Dirac system, the chemically modified TI top layer needs to be removed gently, in order to access the Dirac system. In well-fabricated S-TI-S junctions a strong superconducting proximity effect can facilitate a dissipationless supercurrent. Applying a gentle Ar^+-etch right before the Nb deposition led to good results. Although researchers achieved high quality interfaces in such S-TI-S junctions [10–13], signatures of MBS have only been observed in (Bi,Sb)-based S-TI-S junctions, which had their weak link capped by a stoichiometric Al_2O_3 capping layer [5]. Here, we exploit a native AlO_x-capping for the purpose of conserving the TI surface *in situ*. One advantage of a native oxide is the fact that it can be removed wet chemically in a very controlled and straightforward manner. This makes it possible to define electrodes *ex situ*, which, in return, makes magnetic field control of as-prepared topological devices possible, while assuring an *in situ* capped weak link.

2. Sample preparation

The junctions presented here have been fabricated from a topological heterostructure of nominal 6 nm Bi_2Te_3 and 15 nm Sb_2Te_3 (Fig. 1b). Before transferring the substrate – a 4″ Si (1 1 1) wafer – to the molecular beam epitaxy chamber for TI thin film growth, the wafer was cleaned by a standard RCA-procedure [14]. After terminating the dangling bonds of the Si (1 1 1) substrate with Te atoms by means of molecular beam epitaxy, 6 nm Bi_2Te_3 was grown. While keeping the Te flux steady, the Bi shutter was closed and the Sb shutter was opened. By doing so, the desired heterostructure was obtained. After the successful growth of TI, all shutters were closed, the substrate was cooled down to $T_{Sub} = 25\,^{\circ}C$ and the Al effusion cell was ramped up to its operating temperature of $T_{Al} = 1100\,^{\circ}C$ An Al capping layer with a nominal thickness of 3 *nm* was deposited. By exposing the sample to ambient conditions the thin Al layer oxidized and formed a native AlO_x layer [7,15,16].

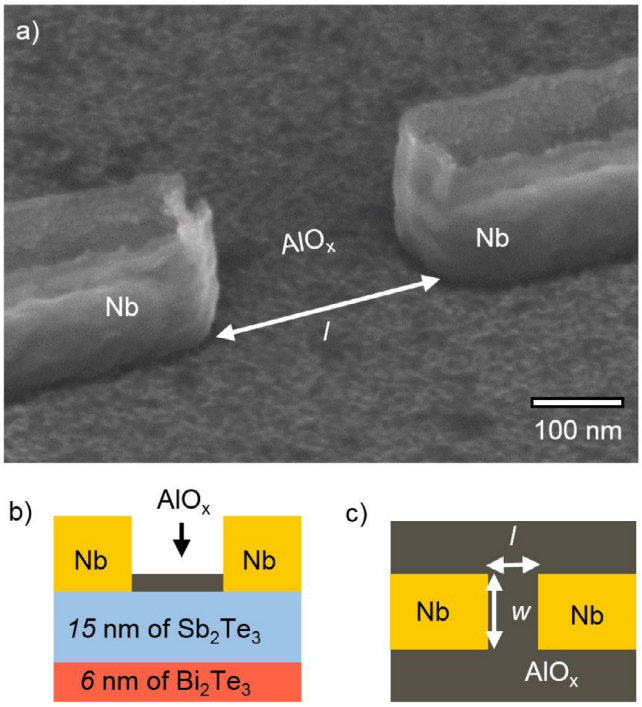

Fig. 1. Lateral S-TI-S junction: a) Scanning electron micrograph of an S-TI-S device defined on top of an extended topological thin film. The surface of the TI thin film is covered by a global AlO_x capping, which protects the TI surface from oxidation. b) Schematic cross-section of the junction. A topological heterostructure (see text) serves as weak link. The area in between the electrodes is capped, while the capping was wet-chemically removed below the Nb electrodes. c) Schematic top view of a junction indicating width (w) and length (l) of the device.

When searching for Majorana signatures in topological hybrid systems, it is mandatory to tune the Fermi level of the TI close to the Dirac point [17,18]. By using n-type Bi_2Te_3 as a pseudo substrate for the subsequent growth of p-type Sb_2Te_3 [19], it is possible to shift the position of the Fermi level of the upper surface as a function of the Sb_2Te_3 layer thickness [20]. Eschbach et al. showed that the top surface of a heterostructure comprised of 6 nm Bi_2Te_3 and 15 nm Sb_2Te_3 has its Fermi level as close as 30 mev to the Dirac point. The associated small Fermi wavelength [18] reduces the number of contributing 2π-periodic Andreev bound states (ABS) [21] and thereby enhances the relative contribution of the exotic 4π-periodic MBS, which superimpose in topological JJs [5,22]. Alternatively, it is possible to tune the Fermi level via alloying of binary Sb_2Te_3 with Bi [18]. However, local variations of Bi/Sb concentration in ternary compounds [23] motivated us to follow the approach of Eschbach et al. [20].

For device fabrication, the AlO_x hard capping needs to be removed thoroughly within the areas in which the electrodes are defined, but it has to remain elsewhere. The capping in the weak link area needs to survive the wet etch in particular. Although there are several etchants for native oxides, alkaline developers hold the advantage that they do not dissolve the electron beam resist, which defines the electrodes. A 120 s bath in OPD-4262 from Fujifilm removed the AlO_x within the area of the electrodes and did not desolve the PMMA mask, resulting in a global capping elsewhere (Fig. 1a). The wet etch was performed immediately before the sputter deposition to minimize the exposure to air before metallization. Before depositing 60 nm of Nb (nominally) in a magnetron sputter chamber at a DC power of 250 W, the sample was gently cleaned via a 30 s Ar^+ plasma etch to remove residual oxides, which might have formed between the AlO_x removal and mounting of the sample in the sputter tool.

In this way, a variety of S-TI-S junctions of different lengths (l) and widths (w) were fabricated. Each device thereby consists of two closely separated Nb electrodes on top of a macroscopic topological thin film (Fig. 1a). The extended thin film assures non-gapped topological surface states within the weak link for arbitrary w of the electrodes. As a result it should be possible to reduce 2π-periodic ABS in narrow junctions significantly without risking a gap opening due to TI confinement [24]. Note that the number of 2π-periodic ABS is proportional to the width of the junction [21]. The difference in dimensions of our junctions should allow for gradually varying the contribution of 2π-periodic ABS, once stable supercurrents are induced.

3. Transport measurements

Three S-TI-S junctions – $S1$ ($w = 2000$ nm, $l = 160$ nm), $S2$ ($w = 400$ nm, $l = 90$ nm) and $S3$ ($w = 100$ nm, $l = 40$ nm) – were wire bonded and subsequently cooled down in an dilution refrigerator. At base temperature (25 mK) we measured the current voltage (I–V) characteristic and the differential resistance (dV/dI) via standard lock-in technology. For directly measuring the voltage drop across the weak link, 4-point measurements were performed. One pair of wires was used to induce a DC + AC signal ($I = I_{bias} + I_{AC}$), while the other pair was used to probe the voltage (V) across the electrodes (insert in Fig. 2a). However, I–V measurements of sample 1 ($S1$) did not show a supercurrent, instead, they only showed a region with a reduced resistance for currents $-25nA \leq I_{bias} \leq 25nA$ (Fig. 2a). By measuring $dV/dI\,(I_{bias})$, the minimum of the resistance at zero I_{bias} was found to be at 45 Ω

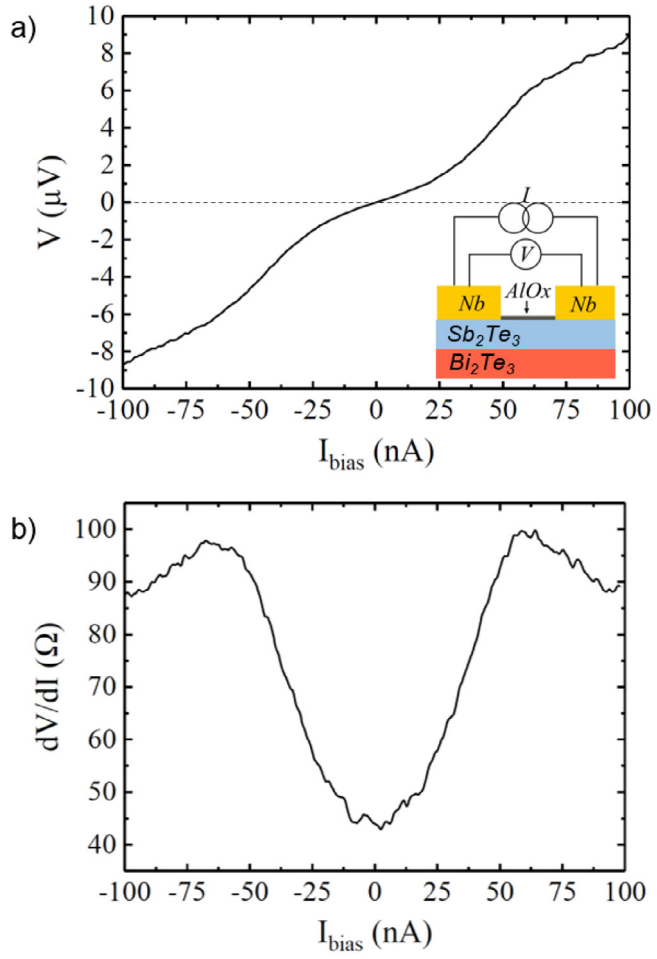

Fig. 2. Low temperature measurements (25 mK), performed on junction $S1$: a) I–V curve: A modulation of the I–V slope is visible for small I_{bias}. b) Differential resistance (dV/dI) as a function of I_{bias}: A zero bias anomaly (ZBA) indicates transport across the TI-S interface via Andreev reflections (see text).

(Fig. 2b), which is approximately half of the normal resistance $R_N = 82\,\Omega$ at high biases (not shown). Such zero bias anomalies (ZBAs) have been observed before [25] and indicate transport across the S-TI interface via Andreev reflections (AR) [26]. Weak links comprised of 3D materials usually show weak ZBAs [27]. ZBAs in 2D electron gases or Dirac systems, however, are expected to show more pronounced ZBAs, since the complete 2D system underneath an electrode is in physical contact with S and therefore fully proximitized. The lack of a supercurrent, however, indicates a low interface transparency between Nb and TI, causing a very small proximity induced gap in the Dirac system below each electrode. To test whether coherent multiple ARs contribute to the current, one can vary the phase difference (φ) across the junction. An increasing perpendicular magnetic field changes φ locally, which in turn periodically varies the net current mediated via coherent Andreev states [28].

Although a stable supercurrent is absent in $S1$, signatures in transport as a function of magnetic field (B) could be ascribed to the periodicity of the expected Fraunhofer-like pattern [11,25] and therefore indicate contributions of coherent Andreev states: By increasing B, the signatures of the ZBA become less pronounced, for magnetic fields up to $B = 1.0\,\text{mT}$ (Fig. 3b). For fields beyond $B = 1.0\,\text{mT}$ the ZBA starts becoming more pronounced again and a clear minimum around zero bias in $dV/dI\,(I_{bias})$ is restored. The periodic change can clearly be seen in the color plot in Fig. 3d). Here, color encodes the differential resistance for varying B and I_{bias}. $dV/dI\,(I_{bias})$ line scans shown in (b) are indicated by vertical lines in (d). A line scan along zero I_{bias} (horizontal red line in Fig. 3d) allows us to extract the minima in B with an averaged periodicity of $B = \Delta 1.2\,\text{mT}$ (Fig. 3c). Our results are in good agreement with measurements of other groups [11,25]. One can relate the periodicity in $dV/dI(B)$ to the area of the junction. The magnetic flux penetrating the weak link can be expressed in terms of $n * \Phi_0$, with $\Phi_0 = h/2e$ being the flux quantum and n an integer number. As soon as one flux quantum is penetrating the junction, left and right-moving currents, which are mediated via coherent Andreev states, should cancel out and a maximum in $dV/dI(B)$ can be observed (Fig. 3c). The corresponding magnetic field allows to calculate the effective area (A_{eff}) of the junction by:

$$B_{1.Max} * A_{eff} = \Phi_0 \tag{1}$$

Magnetic flux-focusing needs to be considered when calculating the effective area [29]. Magnetic flux is screened by the electrodes due to the perfect diamagnetism, which Nb establishes at low temperatures. Field lines, which would penetrate the Nb electrodes in the non-superconducting state, are pushed towards the edge of the electrodes in the superconducting state. Therefore, an additional area (A_{FF}) is also considered, which adds to the geometric area $A_{geo} = l * w$ of the weak link. The additional area A_{FF} includes two triangles, indicated in yellow in Fig. 3a. The shape of the triangles is defined by all points of the superconducting electrode for which the weak link is closer than the side edges. In general, a magnetic field line which penetrates the electrode in the normal (non-superconducting) state will be deflected to the nearest edge in the superconducting state – either to the weak link or to the side edges. Therefore, magnetic field lines that would penetrate the indicated triangles in Fig. 3a will be deflected to the weak link, thus effectively increasing the magnetic flux in between the electrodes. Following [29], the estimated effective area of $S1$ is $A_{\text{eff}} = 2.48\,\mu\text{m}^2$ According to Eq. (1) a periodicity of $\Delta B = 1.2\,\text{mT}$ is expected to occur in $dV/dI(B)$, which is in good agreement with the measurement (Fig. 3c). The measured Fraunhofer-like pattern indicates that the ZBA is sensitive to a change of the superconducting phase difference. This signature represents a precursor of the Josephson effect in our capped topological heterostructures. The reason why the associated Andreev states do not establish a dissipationless supercurrent relates to the ratio of induced gap and electron temperature. Due to a low interface transparency between Nb and TI, the induced gap is very small. For junctions with an improved interface quality a dissipationless supercurrent should become observable at base temperature.

Measurements were carried out on S_2 and S_3 as well. For the 400 nm wide junction (S_2) the resistance dropped from $R_N = 160\,\Omega$ to $45\,\Omega$ at zero bias and zero magnetic field (Fig. 4a). The periodicity of the Fraunhofer-like pattern (Fig. 4b) again suits the dimensions of the effective area ($A_{eff} = 0.1\,\mu\text{m}^2$). In this junction, only two side oscillations could be observed before the magnetic field acted as a global pair breaking mechanism on the coherent Andreev states at $B = \pm 50\,\text{mT}$. This trend becomes even more pronounced for the smallest junction. Despite a clear drop from $R_N = 140\,\Omega$ to $70\,\Omega$ at zero field (Fig. 4c), a Fraunhofer-like pattern is absent (Fig. 4d). Such kind of monotonic decrease of the pairing potential is expected for very narrow junctions. In [30], Cuevas et al. solved the two-dimensional Usadel equation for an S-N-S junction in the diffusive limit and found that the formation of vortices within the weak link is not favorable for a junction in the narrow junction limit. As a consequence, no Fraunhofer-like pattern should be visible. Experimental results support those calculations [31,32].

In $S3$ the field acts solely as pair-breaking mechanism, which suppresses the coherent transport across the junction monotonously. The decrease in resistance at zero bias in all three junctions suggests that it should be possible to induce a supercurrent even in the narrowest junction, if sufficiently transparent interfaces are engineered. Due to the reduced widths of the electrodes, a supercurrent in the narrow junction should consist of a high contribution of 4π-periodic MBS, which are detectable in Shapiro response experiments [33–35].

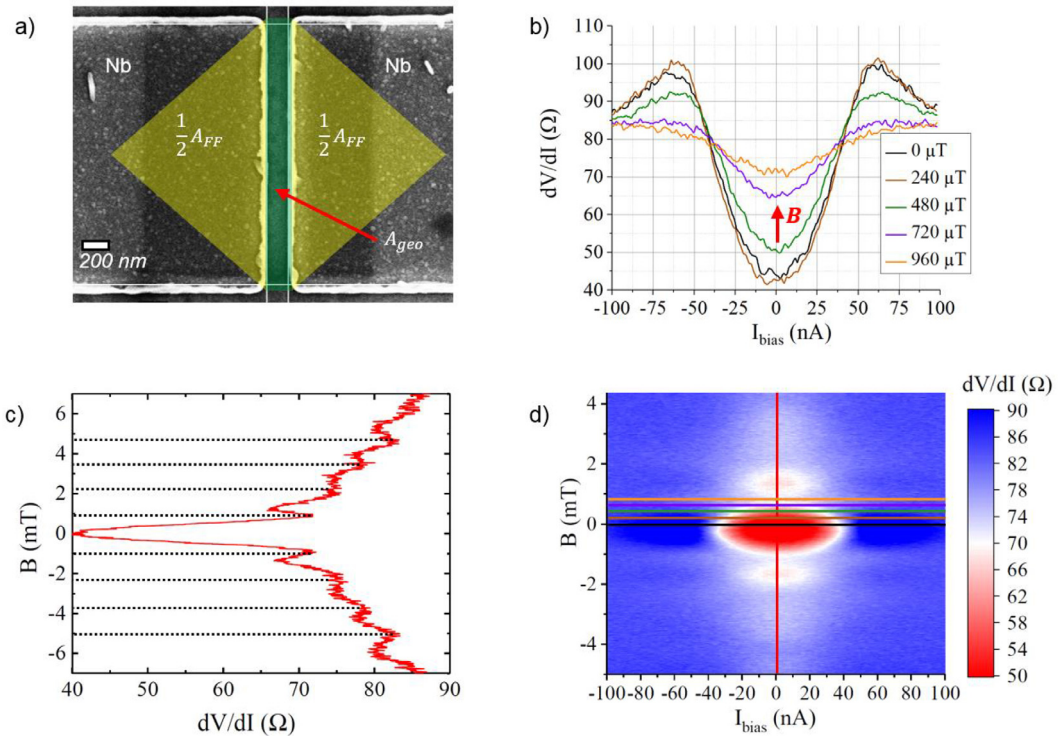

Fig. 3. Magnetic field dependency of *S*1: a) False color SEM image of *S*1: The colored areas are related to the effective area ($A_{eff} = A_{geo} + A_{FF}$) of the junction (see text). The sum of A_{geo} (geometric area) and A_{FF} (area, due to flux focusing) are indicated. b) $dV/dI(I_{bias})$*s* for various magnetic fields. The ZBA becomes less pronounced for increasing *B* fields below 1 mT. c) $dV/dI(B)$ for zero I_{bias}. The oscillations in *B* are related to coherent Andreev states. The periodicity is proportional to the effective area (see text). d) $dV/dI(I_{bias}, B)$: The main minima and the two first side minima are clearly visible (red). For highly transparent interfaces, those minima would drop to zero resistance, yielding a Fraunhofer pattern. Since the junctions did not turn superconductive, the pattern is more precisely referred to as "Fraunhofer-like"-pattern. (For interpretation of the references to color in this figure legend, the reader is referred to the web version of this article.)

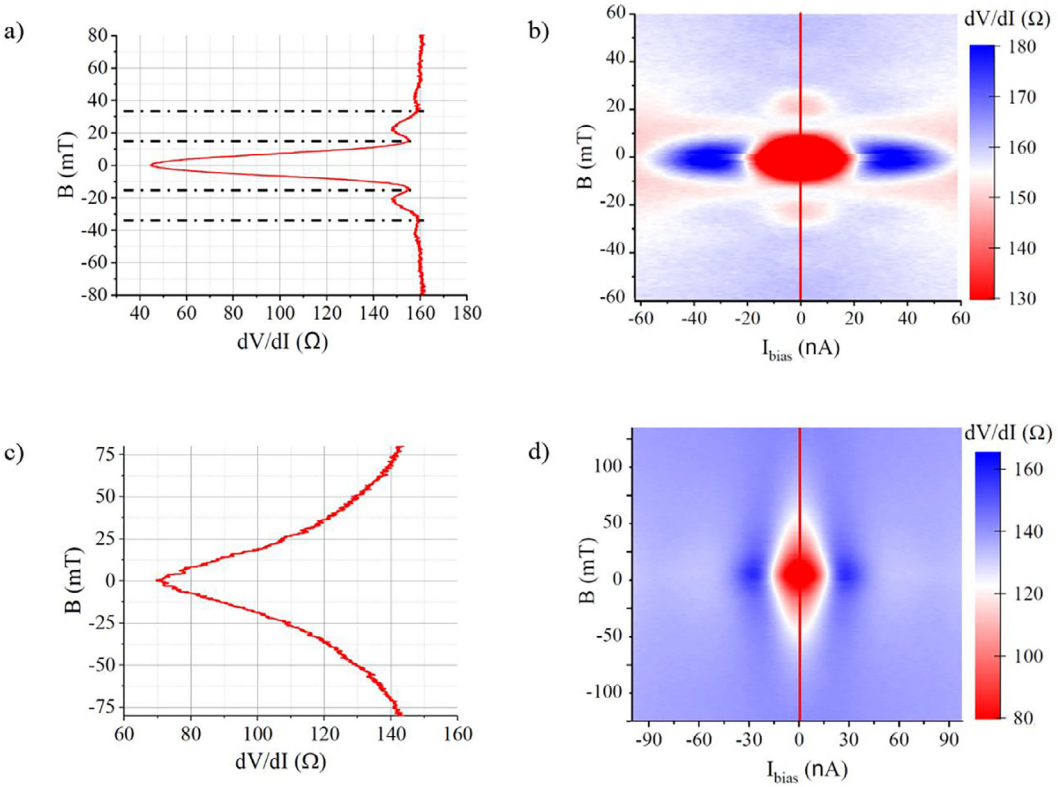

Fig. 4. Magnetic field dependency of *S*2 and *S*3: a) $dV/dI(B)$ for zero I_{bias} of *S*2. The 400 nm wide junction yields a lower periodicity, due to a smaller effective area. b) $dV/dI(I_{bias}, B)$ of *S*2: The main minimum and the two first side minima are again clearly visible. c) $dV/dI(B)$ for zero I_{bias} of *S*3. The smallest junction does not show any oscillations in *B*. Due to its small dimensions the junction is in the short junction limit (see text). d) $dV/dI(I_{bias}, B)$ of *S*3.

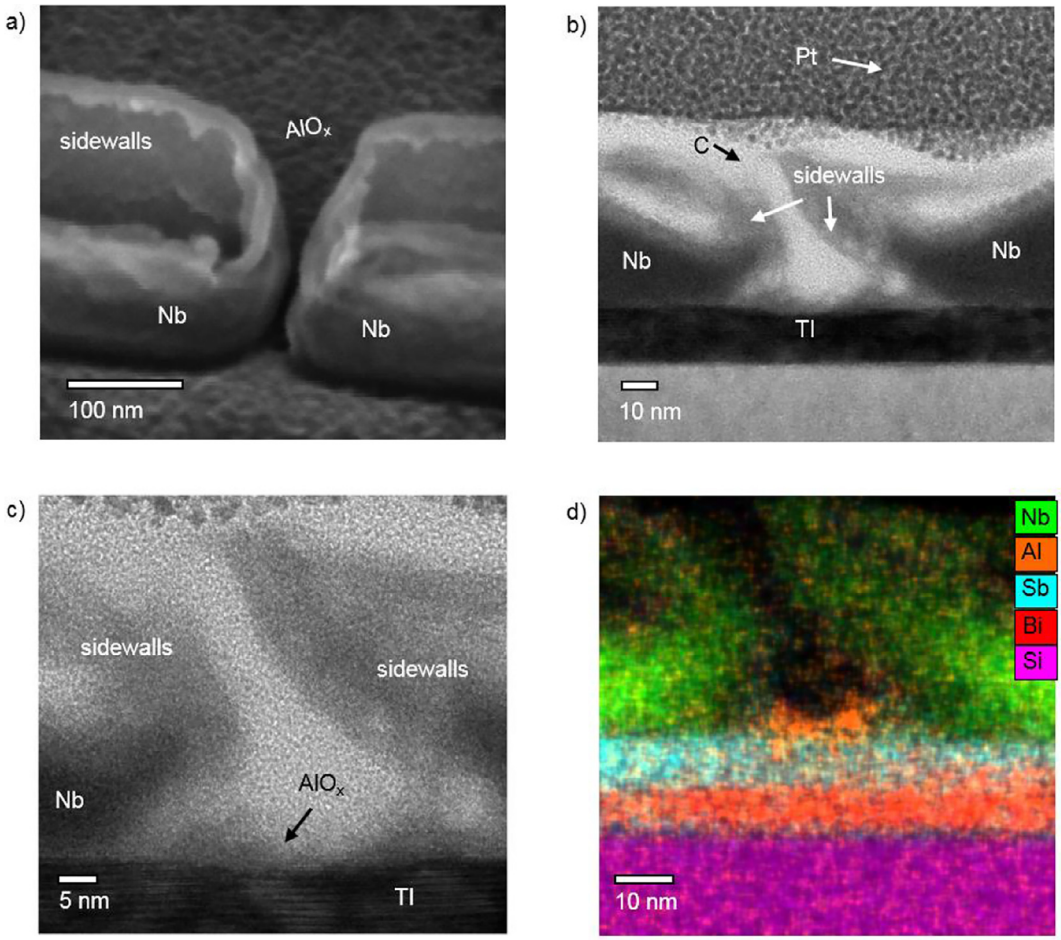

Fig. 5. SEM, TEM and EDX analysis of junction *S*3: a) Perspective SEM image. b) TEM image of the cross-section. c) Close up of (b): The layered crystal is clearly visible. d) EDX map of (c): Bi_2Te_3 and Sb_2Te_3 layers are visible and an AlO_X capping in the weak link area is still present.

4. Transmission electron microscopy analysis

The SEM image in Fig. 5a) displays high sidewalls of resist residuals, which do not allow for a precise estimation of the length of *S*3. Furthermore, it is not possible to see whether or not the weak link is capped. Note that the liquid developer used for AlO_x removal etches isotropically, i.e. lateral etching might remove the AlO_x-capping in very narrow weak links. The transmission electron microscope (TEM) bright field image (Fig. 5b) shows the cross-section of the junction. The height of the superconductive electrodes is reduced in the vicinity of the weak link, forming a 40 nm long junction. During TEM lamella fabrication via FIB the sample was covered with carbon (C) and platinum (Pt). Above the TI layer (dark contrast) the Nb and the sidewalls appear, separated by carbon. A close-up of the weak link region (Fig. 5c) shows the layered crystal of the topological thin film. To understand the local composition, an energy dispersive x-ray (EDX) map has been recorded from the region shown in Fig. 5c). Clearly, Al (orange) can be detected in the weak link area between the Nb electrodes (green), indicating that the AlO_x-capping survived the wet etch even in the narrowest junction (Fig. 5d). Note that the compositional ratio of Bi_2Te_3 and Sb_2Te_3 varies along the cross-section. This variation is presumably due to interdiffusion, caused by heat during fabrication. On the contrary, unprocessed heterostructures show very homogenous element distribution [19].

5. Conclusion

For the fabrication of flux-controllable Majorana devices it is important to a) cap surfaces of (Bi,Sb)-based TIs *in situ* and b) to make devices fabricated from these thin films accessible for external fields. A thin metallic Al layer on top of $(Bi,Sb)_2Te_3$ oxidizes at ambient conditions. The native AlO_x can be preceisely removed locally by OPD-4262 from Fujifilm. This allows for flexible layouts of capped topological devices in the *nm* range. In order to prove the accessibility via external fields, we performed magnetic flux dependent measurements on as-prepared devices. Although a supercurrent was absent in our S-TI-S junctions, clear ZBAs were observed in all devices. The periodicity of dV/dI in a varying B field is in good agreement with the effective area of each junction, which proves a controlled accessibility via magnetic flux. The Fraunhofer-like patterns of the two larger junctions indicate signatures of coherent Andreev states across the weak link. Although the smallest junction is in the narrow junction limit and does not show a Fraunhofer-like pattern, its ZBA is most probably a result of coherent transport, too. Our measurements represent first signatures of induced superconductivity in AlO_x-capped topological S-TI-S junctions. Once the interface transparency between S and TI is optimized and a dissipationless supercurrent is induced, one is able to search for exotic 4π-periodic Majorana modes by performing Shapiro response measurements. Especially in the narrow junction a pronounced 4π-periodic signal is expected, because the number of contributing 2π-periodic ABS should be reduced in the upper surface of Bi_2Te_3-Sb_2Te_3 heterostructures.

Acknowledgements

This work is supported by the Helmholtz Association the “Virtual Institute for Topological Insulators” (VITI).

Appendix A. Supplementary data

Supplementary data to this article can be found online at https://doi.org/10.1016/j.sse.2019.03.003.

References

[1] Kitaev AY. Fault-tolerant quantum computation by anyons. Ann Phys 2003;303(1):2–30.
[2] Kitaev AY. Unpaired Majorana fermions in quantum wires. Phys Usp 2001;44(10S):131.
[3] Cook A, Franz M. Majorana fermions in a topological-insulator nanowire proximity-coupled to an s-wave superconductor. Phys Rev B 2011;84(20):201105.
[4] Cook AM, Vazifeh MM, Franz M. Stability of Majorana fermions in proximity-coupled topological insulator nanowires. Phys Rev B 2012;86(15):155431.
[5] Schüffelgen P, Rosenbach D, Chuan L, Schmitt T, Schleenvoigt M, Jalil AR, et al. Boosting transparency in topological josephson junctions via Stencil Lithography. ArXiv 2017. 1711.01665.
[6] Hyart T, van Heck B, Fulga IC, Burrello M, Akhmerov AR, Beenakker CWJ. Flux-controlled quantum computation with Majorana fermions. Phys Rev B. 2013;88(3):035121.
[7] Lang MR, He L, Xiu FX, Yu XX, Tang JS, Wang Y, et al. Revelation of Topological surface states in Bi2Se3 Thin Films by In Situ Al passivation. ACS Nano 2012;6(1):295–302.
[8] Benia HM, Lin C, Kern K, Ast CR. Reactive chemical doping of the Bi_2Se_3 topological insulator. Phys Rev Lett 2011;107(17):177602.
[9] Chen C, He S, Weng H, Zhang W, Zhao L, Liu H, et al. Robustness of topological order and formation of quantum well states in topological insulators exposed to ambient environment. Proc Natl Acad Sci 2012;109(10):3694–8.
[10] Williams JR, Bestwick AJ, Gallagher P, Hong SS, Cui Y, Bleich AS, et al. Unconventional josephson effect in hybrid superconductor-topological insulator devices. Phys Rev Lett 2012;109(5):056803.
[11] Oostinga JB, Maier L, Schüffelgen P, Knott D, Ames C, Brüne C, et al. Josephson supercurrent through the topological surface states of strained bulk HgTe. Phys Rev X 2013;3(2):021007.
[12] Veldhorst M, Snelder M, Hoek M, Gang T, Guduru VK, Wang XL, et al. Josephson supercurrent through a topological insulator surface state. Nat Mater 2012;11:417.
[13] Yang F, Qu F, Shen J, Ding Y, Chen J, Ji Z, et al. Proximity-effect-induced superconducting phase in the topological insulator Bi2Se3. Phys Rev B 2012;86(13):134504.
[14] Krumrain J, Mussler G, Borisova S, Stoica T, Plucinski L, Schneider CM, et al. MBE growth optimization of topological insulator Bi2Te3 films. J Cryst Growth 2011;324(1):115–8.
[15] Ngabonziza P, Stehno MP, Myoren H, Neumann VA, Koster G, Brinkman A. Gate-tunable transport properties of in situ capped Bi2Te3 topological insulator thin films. Adv Electron Mater 2016;2(8).
[16] Schüffelgen P, Rosenbach D, Neumann E, Stehno MP, Lanius M, Zhao J, et al. Stencil lithography of superconducting contacts on MBE-grown topological insulator thin films. J Cryst Growth 2017;477:183–7.
[17] Snelder M, Molenaar CG, Pan Y, Wu D, Huang YK, Visser Ad, et al. Josephson supercurrent in a topological insulator without a bulk shunt. Supercond Sci Technol 2014;27(10):104001.
[18] Kellner J, Eschbach M, Kampmeier J, Lanius M, Mlynczak E, Mussler G, et al. Tuning the Dirac point to the Fermi level in the ternary topological insulator (Bi1-xSbx)2-Te3. Appl Phys Lett 2015;107(25).
[19] Lanius M, Kampmeier J, Weyrich C, Kolling S, Schall M, Schüffelgen P, et al. P-N junctions in ultrathin topological insulator Sb2Te3/Bi2Te3 heterostructures grown by molecular beam epitaxy. Cryst Growth Des 2016;16(4):2057–61.
[20] Eschbach M, Mlynczak E, Kellner J, Kampmeier J, Lanius M, Neumann E, et al. Realization of a vertical topological p-n junction in epitaxial Sb2Te3/Bi2Te3 heterostructures. Nat Commun 2015:6.
[21] Beenakker CWJ, van Houten H. Quantum Transport in Semiconductor Nanostructures. In: Ehrenreich H, Turnbull D, editors. Solid State Physics. Academic Press; 1991. p. 1–228.
[22] Domínguez F, Kashuba O, Bocquillon E, Wiedenmann J, Deacon RS, Klapwijk TM, et al. Josephson junction dynamics in the presence of 2π and 4π-periodic supercurrents. Phys Rev B 2017;95(19):195430.
[23] Weyrich C, Drögeler M, Kampmeier J, Eschbach M, Mussler G, Merzenich T, et al. Growth, characterization, and transport properties of ternary (Bi 1–x Sb x) 2 Te 3 topological insulator layers. J Phys: Condens Matter 2016;28(49):495501.
[24] Bardarson JH, Brouwer PW, Moore JE. Aharonov-Bohm oscillations in disordered topological insulator nanowires. Phys Rev Lett 2010;105(15):156803.
[25] Maier L, Oostinga JB, Knott D, Brune C, Virtanen P, Tkachov G, et al. Induced superconductivity in the three-dimensional topological insulator HgTe. Phys Rev Lett 2012;109(18).
[26] Pannetier B, Courtois H. Andreev reflection and proximity effect. J Low Temp Phys 2000;118(5):599–615.
[27] Klapwijk TM. Proximity effect from an andreev perspective. J Supercond 2004;17(5):593–611.
[28] Gross R, Festkörperphysik Marx A. De Gruyter Studium 2014.
[29] Molenaar CG, Leusink DP, Wang XL, Brinkman A. Geometric dependence of Nb-Bi 2 Te 3 -Nb topological Josephson junction transport parameters. Supercond Sci Technol 2014;27(10):104003.
[30] Cuevas JC, Bergeret FS. Magnetic interference patterns and vortices in diffusive SNS junctions. Phys Rev Lett 2007;99(21):217002.
[31] Angers L, Chiodi F, Montambaux G, Ferrier M, Guéron S, Bouchiat H, et al. Proximity dc squids in the long-junction limit. Phys Rev B 2008;77(16):165408.
[32] Günel Y. The absence of Fraunhofer patterns in narrow Nb/InAs-nanowire/Nb junctions. AIP Conf Proc 2013;1566(1):109–10.
[33] Li C, de Boer JC, de Ronde B, Ramankutty SV, van Heumen E, Huang Y, et al. 4π-periodic Andreev bound states in a Dirac semimetal. Nat Mater 2018;17(10):875–80.
[34] Bocquillon E, Deacon RS, Wiedenmann J, Leubner P, Klapwijk TM, Brune C, et al. Gapless Andreev bound states in the quantum spin Hall insulator HgTe. Nat Nanotechnol 2017;12(2):137–43.
[35] Wiedenmann J, Bocquillon E, Deacon RS, Hartinger S, Herrmann O, Klapwijk TM, et al. 4π-periodic Josephson supercurrent in HgTe-based topological Josephson junctions. Nat Commun 2016(7).

Peter Schüffelgen received his diploma from the University of Wuerzburg, where he worked on induced superconductivity in HgTe. After finishing his Ph.D. at the RWTH Aachen, he continued his work on Majorana physics and devices at Forschungszentrum Jülich GmbH as post-doctoral scientist. He is currently setting up his own junior investigators group in the field of topological quantum computation and a quantum technology laboratory in the Peter Grünberg Institute 9.